Quantifying transcription factor–DNA binding in single cells *in vivo* with photoactivatable fluorescence correlation spectroscopy

Ziqing Winston Zhao[1,3], Melanie D White[1,3], Yanina D Alvarez[1–3], Jennifer Zenker[1,3], Stephanie Bissiere[1] & Nicolas Plachta[1]

[1]Institute of Molecular and Cell Biology (IMCB), Agency for Science, Technology and Research (A*STAR), Singapore, Singapore. [2]Facultad de Ciencias Exactas y Naturales, Universidad de Buenos Aires, Consejo Nacional de Investigaciones Científicas y Técnicas (CONICET), Buenos Aires, Argentina. [3]These authors contributed equally to this work. Correspondence should be addressed to N.P. (plachtan@imcb.a-star.edu.sg).

Published online 29 June 2017; doi:10.1038/nprot.2017.051

Probing transcription factor (TF)–DNA interactions remains challenging in complex *in vivo* systems such as mammalian embryos, especially when TF copy numbers and fluorescence background are high. To address this difficulty, fluorescence correlation spectroscopy (FCS) can be combined with the use of photoactivatable fluorescent proteins to achieve selective photoactivation of a subset of tagged TF molecules. This approach, termed paFCS, enables FCS measurements within single cell nuclei inside live embryos, and obtains autocorrelation data of a quality previously only attainable in simpler *in vitro* cell culture systems. Here, we present a protocol demonstrating the applicability of paFCS in developing mouse embryos by outlining its implementation on a commercial laser-scanning microscope. We also provide procedures for optimizing the photoactivation and acquisition parameters and determining key parameters describing TF–DNA binding. The entire procedure can be performed within ~2 d (excluding embryo culture time), although the acquisition of each paFCS data set takes only ~10 min. This protocol can be used to noninvasively reveal cell-to-cell variation in TF dynamics, as well as critical, fate-predicting changes over the course of early embryonic development.

INTRODUCTION

TFs interact with DNA to regulate gene expression and cell differentiation. Such interactions, which have long been known to be highly dynamic[1], represent the first layer of transcriptional regulation in eukaryotes. Despite recent progress in probing TF–DNA binding dynamics in cell culture systems[2–15], it remains challenging to study these processes in more *in vivo* contexts, such as in living mammalian embryos over the course of their development. Here, we present a detailed protocol based on paFCS to quantitatively probe the DNA-binding dynamics of TFs at the single-cell level in living mouse embryos. This technique could be widely applied to other live embryos or tissues, and the physical insights obtained will shed light on the multiscale landscape of transcriptional regulation in complex *in vivo* systems.

Development of the protocol

FCS comprises a group of related techniques that probe molecular motion by analyzing the intensity fluctuations produced when fluorescent molecules move in and out of a small observation volume. Autocorrelation analysis of these fluctuation traces provides quantitative information on the dynamics of these molecules. Since its initial development in 1972 (ref. 16), FCS has become a powerful biophysical technique for probing a wide range of dynamic processes in living systems[17–20], and a variety of protocols detailing the application of FCS and related techniques, primarily in cultured cells, have become available in recent years[21–24]. However, the utility of these techniques is often limited by the high abundance of biomolecules typically present in mammalian cells. For example, gene-regulatory proteins such as TFs are typically present at thousands of copies or more within a mammalian cell nucleus[25]. If the entire cellular pool of a TF is fluorescent during FCS measurements, the high fluorescence background causes deterioration of the signal-to-noise (S/N) ratio and hampers the accurate fitting of autocorrelation functions (ACFs)[18,19], a critical step in obtaining quantitative properties of TF–DNA interactions, such as the bound fraction and residence time. Although this problem can be minimized by diluting the fluorescent proteins in cell-free assays or by selecting cells displaying the lowest level of fluorescence background in cell culture systems, these approaches are unfeasible in highly complex *in vivo* systems such as developing embryos or live tissues.

To addresses this deficiency, we recently integrated conventional FCS with the use of photoactivatable fluorescent proteins[26] and carefully optimized photoactivation schemes, thereby enabling the number of fluorescent TF molecules detected to be fine-tuned[27]. This technique, termed paFCS, achieves S/N ratios that are superior to those typically attainable using conventional FCS in cultured cells, and expands the applicability of FCS to multicellular *in vivo* contexts. paFCS has been successfully applied to probe the nuclear dynamics of TFs critical to mammalian development, such as Oct4 and Sox2, and has led to discoveries demonstrating that quantitative changes in TF–DNA interactions predict cell differentiation during the earliest stages of embryogenesis[27,28].

Applications of the method

paFCS is an ideal tool for interrogating the dynamics of TF–DNA interactions in a variety of *in vivo* systems. Broadly appealing to any life scientist seeking a quantitative understanding of TF mechanisms, this technique is particularly useful for biophysicists, cell biologists, and developmental biologists exploring the role of protein dynamics in physiological environments, especially beyond cells cultured *in vitro*. In addition to the mouse embryo demonstrated here, paFCS will be applicable to the majority of embryo types used in developmental biology, as well as to live tissues. In addition to TFs, paFCS could also be used to probe the

dynamics of a variety of other DNA-binding proteins, as well as protein–protein interactions *in vivo*.

Comparison with other methods

Among the techniques currently available for quantitatively probing TF dynamics, single-molecule tracking (SMT) possesses the convenience of direct visualization without the need for excessive calibration or correction[29]. However, SMT has been mainly restricted to cultured cell systems, and the relatively short trajectories that can be captured (especially when using fluorescent proteins) can also limit its utility at times. On the other hand, photobleaching-based methods such as fluorescence recovery after photobleaching (FRAP) lack the temporal resolution needed to resolve transient TF dynamics, and their ensemble nature makes them prone to masking intrinsic heterogeneities among individual TF molecules. Although conventional FCS has previously been applied to the study of both intracellular and extracellular proteins in zebrafish embryos[30–32], it remains limited in its ability to probe dynamic processes inside the mammalian cell nucleus (most likely because of the high fluorescence background, as well as the high copy numbers of key molecular players present). On the other hand, although light-sheet-based FCS[33,34] can generate spatially resolved maps of protein dynamics *in vivo*, these schemes are substantially more difficult to implement because of the need for separate illumination optics.

The central advantage of paFCS lies in its applicability to live samples with large axial depth and high fluorescence background. By enhancing the S/N ratio, paFCS is capable of probing single-cell nuclei inside a developing embryo, which are currently not amenable to conventional FCS measurements or other quantitative imaging approaches. The high temporal resolution of paFCS allows researchers to distinguish among different modes of TF–DNA interactions spanning a wider range of time scales (from milliseconds to seconds) than those typically probed using SMT techniques[5]. paFCS also generates less photobleaching and phototoxicity than conventional FCS, making it suitable for probing highly photosensitive samples over a relatively long period of time without perturbing their development. Moreover, the use of confocal excitation during paFCS measurement allows for localized data acquisition, thereby further enabling the investigation of potential spatial heterogeneities in TF dynamics across different regions of the cell nucleus. Finally, paFCS can be simply implemented on any confocal microscope, making it accessible to a wide range of users.

Limitations

One major limitation of paFCS, as is the case for all single-point FCS modalities, lies in its inability to provide spatially resolved dynamic information in a high-throughput manner, unlike other related techniques such as light-sheet-based FCS[33,34] or raster image correlation spectroscopy (RICS)[35]. The dynamic parameters obtained from paFCS are also critically dependent on the choice of the theoretical model used, making data analysis more complicated than that for other model-independent techniques such as pair correlation analysis[36]. The need for calibration also limits its ease of use as compared with line-scanning FCS, which is calibration-free and less sensitive to laser misalignment and optical artifacts[37]. In addition, paFCS is currently incapable of probing highly immobile proteins (e.g., cell surface receptors) as they are especially susceptible to photobleaching during data acquisition, although future combination with light-sheet microscopy and line-scanning approaches may provide new avenues to expand its applicability to these areas. Last, only the use of paGFP for tagging TFs was demonstrated in this protocol, as we found this protein to provide the best S/N ratio and minimal photobleaching during FCS measurements. paGFP can also be efficiently photoactivated within complex 3D specimens, using either an 820-nm laser or a 405-nm laser[38,39], thereby giving users the flexibility to choose the strategy most suitable to their experimental system, especially when multiple molecular species must be imaged simultaneously. However, the continuous development of new photoactivatable and photoconvertible fluorescent proteins with improved spectral properties[40], as well as novel approaches for photoactivation using multiphoton-based excitation[41], may expand the pool of potential fluorescent tags and further enable multiplexed interrogation of different TF–DNA interactions *in vivo*.

Outline of the paFCS workflow

The workflow for performing paFCS measurements on live mouse embryos is outlined in **Figure 1**. After the embryos are harvested, the mRNAs for both the paGFP-tagged TF of interest and a cell nucleus marker (such as H2B-RFP) are co-microinjected into a cell of the embryo at the appropriate developmental stage. The embryos are subsequently allowed to develop in a culture chamber (Steps 1–7). Upon calibration (Steps 8–12) and setup (Steps 13–16) of the microscope and optimization of the photoactivation/acquisition parameters (Steps 17–21), a cell nucleus of the embryo expressing the nuclear marker is photoactivated with either an 820-nm or a 405-nm laser to selectively activate a desired fraction of the TF-paGFP molecules. FCS measurements are then performed at selected locations within the nucleus using a 488-nm laser (Steps 22–26). Subsequently, ACFs are calculated from the raw data and fitted with the appropriate theoretical model functions to extract quantitative parameters such as diffusion coefficients, residence times, and the fractions of bound and free TFs (Steps 27–33). These steps can then be repeated on other embryos, either at different stages of development or treated with experimental perturbations, such as drugs or expression of mutant forms of the TF that perturb DNA binding.

Experimental design

Calibration of the confocal volume. The accuracy of FCS measurements relies on the precise determination of the confocal volume, or the point spread function (PSF) of the confocal microscope used. The PSF has a complicated ellipsoidal profile that depends on the excitation and collection optics, but for FCS measurements it can be reasonably described by a 3D Gaussian distribution

$$I(x,y,z) = I_0 \exp\left[-\frac{2(x^2+y^2)}{r_0^2}\right]\exp\left(-\frac{2z^2}{z_0^2}\right) \quad (1)$$

where r_0 denotes the transverse waist of the confocal volume and z_0 the axial waist[42]. The effective confocal volume V_{eff} can then be calculated as

$$V_{\text{eff}} = \pi^{3/2} r_0^2 z_0 = \pi^{3/2} r_0^3 \omega \quad (2)$$

where ω is the structural parameter of the confocal volume defined as $\omega = z_0/r_0$. To detect any deviation that could arise in the system over time, periodical checking of the size and shape of the confocal volume should be performed, either by taking measurements from images of subresolution-sized fluorescent beads or by using a solution of a fluorescent dye with a known diffusion coefficient (see Step 12).

Optimization of photoactivation and paFCS acquisition parameters. One of the key steps of paFCS that enables the acquisition of ACFs with superior S/N ratios is the selective photoactivation of an appropriately small fraction of the TF population within the cell nucleus. Given the varying levels of expression of different TFs, as well as the nuclear environment of the *in vivo*

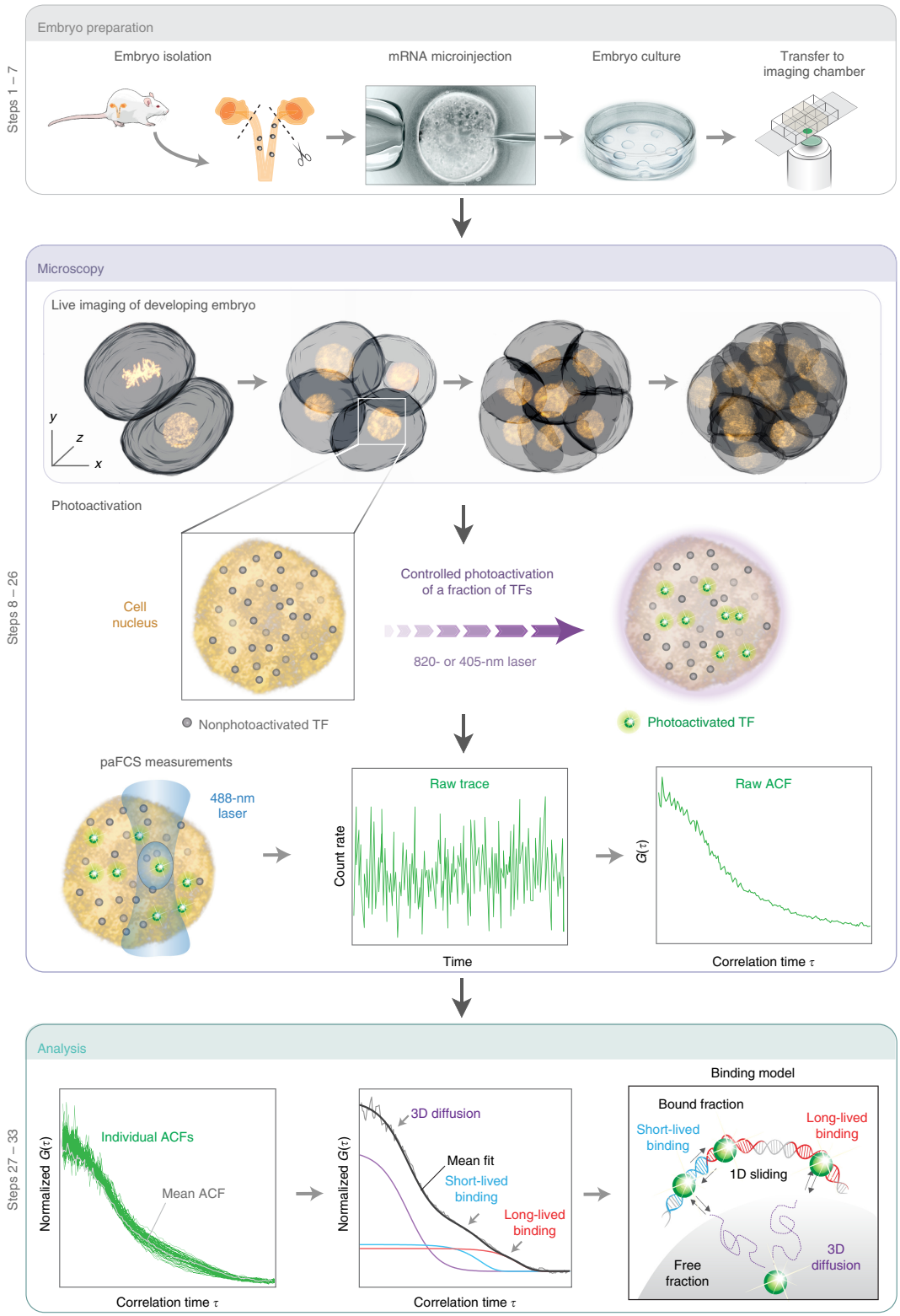

Figure 1 | paFCS workflow. *G*, autocorrelation function.

system of choice, the parameters of the photoactivation step must be carefully optimized for each TF and model system before the acquisition of paFCS data. Preferably, the photoactivation should be performed using an 820-nm multiphoton laser; alternatively, a 405-nm laser could also be used, although such usage may result in considerable photoactivation above and below the desired axial plane. The parameters of the photoactivation scheme that can be fine-tuned include laser intensity, pixel dwell time (typically adjusted via scanning speed), and the number of photoactivation iterations used. Similarly, the laser intensity used for FCS data acquisition must also be carefully optimized to prevent photobleaching and phototoxicity (see Steps 17–21). The ultimate goal of the optimization process is to obtain ACFs with the best S/N ratio possible without any photobleaching-related artifacts, thereby allowing the accurate determination of the various parameters of TF dynamics.

To maximize the statistical significance of the experimental results, it is recommended that as much paFCS data as possible be collected from each cell nucleus. Instead of performing a single long measurement, it is advantageous to perform several repetitions of shorter measurements to allow for the possible exclusion, from final averaging, of traces exhibiting abnormalities such as those associated with photobleaching or sudden movement of intranuclear structures. Typically, the duration of each measurement should exceed at least 1,000-fold the diffusion time of the slowest component exhibited by the TF. For freely diffusing proteins, a 10-s acquisition time is typically sufficient, whereas for a TF exhibiting binding interactions, acquisition times between 10 and 60 s are recommended. A total of 5–10 FCS measurements can be acquired at each intranuclear position; these can then be averaged to further enhance the S/N ratio.

Model selection for fitting paFCS data. Modeling is a critical step in extracting quantitative information on TF dynamics from the experimental paFCS data. Here we outline some of the key considerations in analyzing paFCS data and choosing the most appropriate model for fitting.

In many fluorescent proteins (including GFP), a variety of fast photophysical processes can take place on the microsecond time scale[43]. Chief among them is the contribution from triplet-state formation, a process through which the fluorophore transitions from an excitable singlet state to a quenched triplet state, which occurs on time scales between 1 and 10 µs. This, together with other fast processes such as protonation/deprotonation and isomerization, gives rise to multiple components in the overall ACF. Given the separation of their time scales from that of intracellular protein diffusion, which usually occurs on a submillisecond time scale, these contributions can be grouped into a single term denoted by $G_{\text{triplet}}(\tau)$. The overall ACF can then be expressed as a product of $G_{\text{triplet}}(\tau)$ and the correlation function arising from TF dynamics, $G_{\text{TF}}(\tau)$:

$$G(\tau) = G_{\text{TF}}(\tau)G_{\text{triplet}}(\tau) = G_{\text{TF}}(\tau)\left[1 + \frac{F_t}{1-F_t}\exp\left(-\frac{\tau}{\tau_t}\right)\right] \quad (3)$$

where F_t and τ_t denote the fraction of molecules in the triplet state (as well as other transient states) and the characteristic time associated with these states, respectively.

Given that a TF molecule often exhibits more than one mode of diffusion in the nucleus (i.e., free, super-, and sub-diffusion), models used to fit ACFs usually consist of at least two components in $G_{\text{TF}}(\tau)$ to account for the various subpopulations. The ACF for the simplest case, that of free diffusion of a fluorescent molecule in a 3D Gaussian PSF, can be written as

$$G_{\text{TF}}(\tau) = \frac{1}{N}\left(1 + \frac{\tau}{\tau_D}\right)^{-1}\left(1 + \frac{\tau}{\omega^2\tau_D}\right)^{-1/2} \quad (4)$$

where N is the average number of fluorescent molecules within the confocal volume, ω is the structural parameter as previously defined, and τ_D is the correlation time for free diffusion defined as $\tau_D = r_0^2/4D$, with D being the diffusion coefficient of the TF and r_0 being the radial waist of the confocal volume. Given that movement in the crowded nuclear environment is often constrained by interactions with chromatin or other proteins, an anomalous diffusion model may better account for the TF dynamics. The ACF in this case can be expressed as

$$G_{\text{TF}}(\tau) = \frac{1}{N}\left(1 + \left(\frac{\tau}{\tau_{AD}}\right)^{\alpha}\right)^{-1}\left(1 + \frac{1}{\omega^2}\left(\frac{\tau}{\tau_{AD}}\right)^{\alpha}\right)^{-1/2} \quad (5)$$

where τ_{AD} is the correlation time for anomalous diffusion similarly defined as τ_D, and α is an anomaly parameter that measures the deviation from purely free diffusion, for which $\alpha = 1$. The diffusion is termed super-diffusion when $\alpha > 1$, and sub-diffusion when $\alpha < 1$ (ref. 44). The ACF for models consisting of two components can then be expressed as a sum of the ACFs for each component, weighted by their respective molecular fractions. For example, when the model consists of two free diffusive components (one slow and one fast) or one fast free component and one slow anomalous component, the ACF can be, respectively, written as

$$G_{\text{TF}}(\tau) = \frac{F_D^{\text{fast}}}{N}\left(1 + \frac{\tau}{\tau_D^{\text{fast}}}\right)^{-1}\left(1 + \frac{\tau}{\omega^2\tau_D^{\text{fast}}}\right)^{-1/2} + \frac{F_D^{\text{slow}}}{N}\left(1 + \frac{\tau}{\tau_D^{\text{slow}}}\right)^{-1}\left(1 + \frac{\tau}{\omega^2\tau_D^{\text{slow}}}\right)^{-1/2} \quad (6)$$

$$G_{\text{TF}}(\tau) = \frac{F_D^{\text{fast}}}{N}\left(1 + \frac{\tau}{\tau_D^{\text{fast}}}\right)^{-1}\left(1 + \frac{\tau}{\omega^2\tau_D^{\text{fast}}}\right)^{-1/2} + \frac{F_{AD}^{\text{slow}}}{N}\left(1 + \left(\frac{\tau}{\tau_{AD}^{\text{slow}}}\right)^{\alpha}\right)^{-1}\left(1 + \frac{1}{\omega^2}\left(\frac{\tau}{\tau_{AD}^{\text{slow}}}\right)^{\alpha}\right)^{-1/2} \quad (7)$$

In addition to diffusion, TFs carry out their regulatory functions by binding to chromatin DNA, a process that can be modeled as a first-order reversible reaction:

$$TF_{\text{free}} \underset{k_{\text{off}}}{\overset{k_{\text{on}}}{\rightleftharpoons}} TF_{\text{bound}} \quad (8)$$

where TF_{free} and TF_{bound} denote the free and bound states of the TF, respectively, and k_{on} and k_{off} are the association and disassociation rate constants, respectively. Experimentally, the observed

association rate takes into account both k_{on} and the total concentration of DNA-binding sites, and is usually denoted as k^*_{on}. The inverse of k^*_{on} then gives the average time a TF molecule takes to find its target site, whereas the inverse of k_{off} gives the average residence time during which the TF molecule stays bound to DNA. The ACF for a TF exhibiting both diffusion and binding, under the assumption that the diffusion time is much shorter than the residence time, can be given by

$$G_{TF}(\tau) = \frac{F_D}{N}\left(1+\frac{\tau}{\tau_D}\right)^{-1}\left(1+\frac{\tau}{\omega^2\tau_D}\right)^{-1/2} + \frac{F_{bound}}{N}e^{-k_{off}\tau} \quad (9)$$

where $F_{bound} = k^*_{on}/(k^*_{on} + k^*_{off})$ denotes the bound fraction[45]. Besides specific binding sites, TF can also bind DNA sites with lower affinity during its target search process. A model that accounts for this possibility therefore includes two binding components with temporally distinct residence times:

$$G_{TF}(\tau) = \frac{F_D}{N}\left(1+\frac{\tau}{\tau_D}\right)^{-1}\left(1+\frac{\tau}{\omega^2\tau_D}\right)^{-1/2} + \frac{F^{short}_{bound}}{N}e^{-k^{short}_{off}\tau} + \frac{F^{long}_{bound}}{N}e^{-k^{long}_{off}\tau} \quad (10)$$

in which the association and dissociation rates and the diffusing and bound fractions are related according to[45]:

$$F_D = \frac{1}{1+\frac{k^{*short}_{on}}{k^{short}_{off}}+\frac{k^{*long}_{on}}{k^{long}_{off}}} \quad (11a)$$

$$F^{short}_{bound} = \frac{k^{*short}_{on}}{k^{short}_{off}}F_D \quad (11b)$$

$$F^{long}_{bound} = \frac{k^{*long}_{on}}{k^{long}_{off}}F_D \quad (11c)$$

It should be pointed out that slow anomalous diffusion should not simply be taken to denote DNA binding without first performing careful validation. One way to do this, for example, is by assessing the effect of changing the observation volume size on the ACF obtained, as the characteristic time of fluorescence fluctuations for diffusing molecules increases with the size of the observation volume, whereas the dwell time resulting from TF binding should be independent of volume size, as it is primarily determined by the unbinding rate[45,46]. Such validation has recently been performed for the mouse TF Sox2 using a line-scanning approach, for which the slow-diffusing component was found to indeed arise from binding events[28]. However, the results of such validation are system-specific, and therefore the choice of the most suitable model to use for fitting the experimental ACF depends on the actual dynamics of the TF, as well as the *in vivo* system under investigation, and requires empirical determination in a nonbiased manner (see Steps 27–32).

Probing quantitative changes in TF-binding dynamics with paFCS. TF–DNA interactions *in vivo* can be perturbed with a variety of factors, and the impact of such perturbations can be quantitatively probed using paFCS. For example, TF dynamics depends on the accessibility of available DNA-binding sites, which can be modulated by globally increasing or decreasing chromatin compaction with drugs such as trichostatin (TSA) or actinomycin D (Act D), respectively[47,48]. These manipulations are likely to result in changes in the bound fractions of the TF. Moreover, the DNA-binding affinity of a particular TF can be manipulated by site-directed mutagenesis or truncation of its DNA-binding domains. Post-translational modifications proposed to regulate the affinity of a TF for defined DNA sequences can also be disrupted by mutations or by downregulating and/or inhibiting the enzymes that deposit these modifications. Such manipulations are likely to cause changes in the TF's residence time on the DNA. In addition, some TFs rely on protein–protein interactions to achieve DNA binding. These interactions can be manipulated by downregulating the TF's binding partner, and may affect its DNA-bound fraction. Last, the impact of fusing paGFP to the TF of interest on the dynamics and functions of the TF also must be carefully checked before proceeding with the other perturbations.

MATERIALS

REAGENTS

- Female mice between 3 and 4 weeks of age (Biological Resource Centre, Agency for Science, Technology and Research (A*STAR) of Singapore, strain FVB/N) ! CAUTION All procedures involving mice described in this protocol were performed in accordance with approval from the Institutional Animal Care and Use Committee (IACUC) under Project No. 151056, and comply with guidelines from the National Advisory Committee for Laboratory Animal Research (NACLAR) of Singapore. Users should seek advice and approval from the appropriate institutional regulatory boards in their own countries regarding proper and ethical handling of animals.
- M2 medium (Sigma-Aldrich, cat. no. M7167)
- EmbryoMax KSOM embryo culture powder (1×) (Millipore, cat. no. MR-020P-5F) ▲ CRITICAL The embryo culture medium should be phenol-red-free to minimize fluorescence background during imaging.
- Sydney IVF hyaluronidase (Cook Medical, cat. no. G26773)
- Mineral oil suitable for mouse embryo culture (Sigma-Aldrich, cat. no. M8410)
- Sodium chloride (NaCl; Sigma-Aldrich, cat. no. S3014)
- EDTA disodium salt solution (Sigma-Aldrich, cat. no. E7889)
- Tris–EDTA buffer solution (Sigma-Aldrich, cat. no. T9285)
- Water, filter-sterilized and suitable for mouse embryo culture (Sigma-Aldrich, cat. no. W1503)
- paGFP plasmid (Addgene, cat. no. 18697)
- H2B-RFP plasmid (Addgene, cat. no. 53745)
- mMESSAGE mMACHINE SP6 transcription kit (Thermo Fisher Scientific, cat. no. AM1340)
- RNeasy Mini Kit (Qiagen, cat. no. 74104)
- TetraSpeck microspheres, 0.1 µm, fluorescent blue/green/orange/dark red (Invitrogen, cat. no. T7279)
- Alexa Fluor 488 NHS ester (Thermo Fisher Scientific, cat. no. A20000)

EQUIPMENT

- Laser-scanning microscope (Zeiss, model no. LSM 780) with ConfoCor3 module (Carl Zeiss), or any other suitable commercial or home-built setup with FCS capability and a temperature-controlled incubation chamber with CO_2 supply ! CAUTION Laser light can cause severe damage to the eye. Always ensure that laser light is shielded from the user, and wear protective eyeglasses with the appropriate optical density (OD) value while working with lasers. Do not look directly into any laser beam.

- A high numerical aperture (NA) objective suitable for FCS (e.g., C-Apochromat 40×/1.2 W Corr M27; Carl Zeiss, cat. no. 421767-9971)
- Dissection microscope with a transmitted light source (Olympus, cat. no. SZX2-ILLB)
- MINC benchtop incubator (Cook Medical, cat. no. G20079)
- Embryo culture dish (Corning, cat. no. 353001)
- FemtoJet 4i electronic microinjector (Eppendorf, cat. no. 5252 000.013)
- Single concave microscope slides, 1-inch × 3-inch (Parco Scientific, cat. no. C17103)
- Nunc Lab-Tek chambered coverglass, 8-well (Thermo Fisher, cat. no. 155411)
- Flaming/brown micropipette puller (Sutter Instrument, cat. no. P-97)
- Microforge (Narishige, cat. no. MF-900)
- Clark borosilicate thin-wall glass capillaries, both with and without filaments (Warner Instruments, cat. nos. GT100TF-15 and CG100T-15)
- FCS data analysis software (e.g., Zen (https://www.zeiss.com/microscopy/us/products/microscope-software/zen-lite.html), SimFCS (http://www.lfd.uci.edu/globals/), PyCorrFit (https://github.com/FCS-analysis/PyCorrFit), QuickFit3 (http://www.dkfz.de/Macromol/quickfit/), FFS Data Processor (http://www.sstcenter.com/software/index.phtml?pageid=idFFSDPFeatures))

REAGENT SETUP

Injection buffer Dissolve 5 mM NaCl and 0.1 mM EDTA in 5 mM Tris–EDTA buffer solution. The injection buffer can be stored at −20 °C for up to 12 months.

PROCEDURE

Embryo isolation, culture and pro-nuclear microinjection ● TIMING ~1 d

1| Before embryo isolation, construct a plasmid containing paGFP fused to the TF of interest, using the paGFP plasmid. Synthesize the mRNAs of the paGFP-tagged TF and of a nuclear marker (e.g., H2B-RFP) with the mMESSAGE mMACHINE SP6 *in vitro* transcription kit, in accordance with the manufacturer's instructions and using linearized plasmids as templates. Purify the mRNAs with the RNeasy Mini Kit, and store the purified mRNAs at –20 °C for up to 6 months. In the experiments described here, we use Sox2 and Oct4 as our TF of interest.

2| Flush embryos at the one-cell stage from the oviduct of the female mouse with a copious amount of M2 medium, and wash with 1 ml of hyaluronidase solution to remove the cumulus cells (see chap. 4 of ref. 49 for more details). Culture the embryos in embryo culture medium at 37 °C and 5% CO_2 in a culture dish covered with mineral oil. Typically, a total of 6–8 embryos can be harvested from each mouse on average.

3| Embryos are normally microinjected at either the one- or the two-cell stage. Before injection, prepare injection pipettes from borosilicate thin-walled glass capillaries using a micropipette puller, and bevel the holding pipette with the microforge (see chap. 7 of ref. 49 for more details). We typically use the following pulling parameters for the injection pipettes: heat, 490; pull, 95; velocity, 75; delay, 60; pressure, 200. The pulled pipette should have an inner diameter of 0.3–0.7 µm at the tip and a 6- to 9-mm taper.

4| Dilute both mRNA constructs in injection buffer to a final concentration of 50 to 150 ng/µl and a final volume of 10 µl. The final concentration must be empirically determined for each TF so as to obtain the most satisfactory photoactivation and S/N ratio during paFCS (see Steps 17–21). Spin the solution at 16,000*g* for 5 min at room temperature (25 °C).

5| Transfer the embryos onto single concave microscope slides containing 6 µl of M2 medium, and cover them with 1 or 2 drops of mineral oil.

6| Inject 1–2 pl of the diluted mRNA constructs into the nucleus of a cell of the embryo using the FemtoJet 4i electronic microinjector attached to a dissection microscope (see chap. 7 of ref. 49 for more details). Multiple constructs tagged with different fluorophores can be injected simultaneously into one nucleus. Repeat the microinjection on as many embryos as needed. We typically inject ~20 embryos per experimental condition to allow for possible embryo death and developmental defects before paFCS measurement.

▲ **CRITICAL STEP** It will be easier to perform the microinjection before the merging of the pro-nuclei, as both the male and female pro-nuclei can be more easily distinguished and targeted.

? TROUBLESHOOTING

7| After microinjection, keep the embryos in a benchtop incubator at 37 °C and 5% CO_2 until suitable expression levels of the fluorescent proteins have been reached (see Steps 16–19), which typically takes 16–24 h.

Microscope calibration ● TIMING ~1 h

▲ **CRITICAL** Although the protocol outlined here is intentionally general so as to be applicable to any microscope system, the following steps refer to the Zeiss LSM 780 model with a ConfoCor3 module. Other microscope models could be set up and calibrated with minor modifications according to their respective operation procedure.

8| Turn on the microscope, lasers, camera, and control software. Wait until the lasers are warmed up and the camera is stabilized.

9| Turn on the temperature control and CO_2 supply for the incubation chamber on the microscope. Wait until the temperature reaches 37 °C and the CO_2 level reaches 5% (both inside the chamber and the on-stage insert).

10| Before each experimental session, adjust the alignment of the pinhole to ensure that the confocal volume of the laser exhibits a 3D Gaussian profile. In commercial microscopes and most home-built systems, this is achieved by first adjusting the confocal pinhole along the *x* and *y* directions and finding the position for which the detector returns maximum fluorescence intensity and/or counts per molecule (CPM). In the vicinity of the optimum position, the intensity as a function of pinhole position should exhibit a Gaussian distribution. The same adjustment is then performed along the *z* axis, although in this direction the optimal position might be harder to pinpoint because of the more extended intensity distribution. (In the ConfoCor3 module, selecting the 'Adjust Pinhole' button in the 'FCS Light Path' menu accomplishes automatic alignment.)
? TROUBLESHOOTING

11| If the objective used has a correction collar, adjust it to obtain the maximum CPM. This compensates for the potentially considerable spherical aberrations introduced by different coverslip thicknesses or refractive index variations in the immersion medium, especially when using high-NA objectives.

12| The calibration of the confocal volume can be accomplished using two methods: (option A) measurement from images of subresolution-sized fluorescent beads, and (option B) measurement of a fluorescent dye solution with a known diffusion coefficient.

(A) Measurement from images of subresolution-sized fluorescent beads

(i) Select a type of fluorescent bead with a diameter below the resolution of the microscope and a fluorescence emission spectrum that can be detected with the same configurations as used for the FCS experiment (e.g., 0.1-µm TetraSpeck microspheres from Invitrogen).

(ii) Apply a 5-µl droplet of the bead suspension to a clean glass slide. If necessary, dilute the suspension so as to obtain a dispersed distribution of the beads on the glass slide (see Step 12A(iv) below), in which individual beads can be clearly discerned. Wait for the droplet to dry, and apply a 10- to 20-µl drop of glycerol as mounting medium.
▲ **CRITICAL STEP** Before applying the suspension, make sure that the beads are uniformly suspended by mixing on a vortex mixer or by sonicating the suspension.

(iii) Cover the glass slide with a coverslip, and seal it with nail polish.

(iv) Acquire an image of the beads on the glass slide, and check that individual beads can be clearly discerned. Record a 3D stack of the beads with an ~50-nm lateral sampling interval and an ~100-nm axial sampling interval, so as to acquire sufficient data to determine the PSF profile with high accuracy. If possible, use the same imaging conditions (e.g., light path setup, laser power, temperature) as used for FCS measurements.

(v) Analyze the fluorescent images of the beads by fitting their lateral and axial profiles with equation (1) to obtain values of r_0 and z_0, and calculate the effective confocal volume using equation (2) (see 'Experimental design').

(B) Measurement of a fluorescent dye solution with a known diffusion coefficient

(i) Choose a robust dye whose fluorescence emission can be detected with the same configurations as used for the FCS experiment (e.g., Alexa Fluor 488 from Thermo Fisher Scientific), and prepare a series of dilutions with concentrations ranging from 1 nM to 1 µM in PBS and a 0.05% concentration of a soft detergent (e.g., Tween 20) to prevent aggregation and surface adhesion. Make sure that the concentration of the detergent used is well below the critical micelle concentration. Store the stock at 4 °C in the dark for up to 1 month.

(ii) Perform FCS measurements on the solutions using a low power for the 488-nm laser, and calculate the ACFs from the corresponding FCS traces. Pick the concentration that yields the best CPM value and correlation amplitude. Be sure to position the focal plane of the objective inside the solution sample during measurement.

(iii) Fit the ACF obtained with equation (4) (for free 3D diffusion) to obtain the values of r_0 and ω, and calculate the effective confocal volume using equation (2).

Setup of the microscope for paFCS ● TIMING ~1.5 h

13| Before imaging, examine the embryos for signs of abnormal development (e.g., fragmentation, lysis, polyploidy, or growth arrest) as a result of the *ex utero* culture process. Use only healthy-looking embryos for subsequent steps.

14| Transfer healthy embryos from the culture dish to a Nunc Lab-Tek chambered cover glass, and place the chamber onto the microscope stage, maintained at 37 °C and 5% CO_2.
▲ **CRITICAL STEP** Leave the embryos on the microscope stage for at least 1 h before performing photoactivation and paFCS measurements. This ensures that the culture medium is well equilibrated with the incubation environment on the microscope and minimizes any potential impact of mechanical perturbations during the transfer process. Also make sure that the chamber is as level on the microscope stage as possible to prevent embryos drifting over time.

15| Set up the light paths for performing paFCS measurements, including the 820- or 405-nm laser line for photoactivation, 488- and 568-nm laser lines for excitation, and filter and dichroic mirrors for both excitation and emission. Set the pinhole to 1 Airy unit.

© 2017 Macmillan Publishers Limited, part of Springer Nature. All rights reserved.

16| Select an embryo showing clear H2B-RFP expression in the cell nuclei, and position it at the center of the field of view. Select the appropriate zoom factor to fill the field of view with the entire embryo (e.g., a 1.7 zoom factor for a 40× 1.2 NA objective). Acquire an image of the embryo using both the 488-nm and 568-nm laser lines at a single focal plane ~3 µm in thickness through the central region of the cell nucleus to be photoactivated. Adjust the laser intensities to obtain a nonsaturating nuclear signal for H2B-RFP fluorescence and a barely discernible signal for paGFP.
? TROUBLESHOOTING

Optimization of photoactivation and acquisition parameters ● TIMING ~30 min
17| First perform a laser power titration to determine the optimal photoactivation parameters. Photoactivation can be performed using either the 820-nm laser (two-photon mode) or the 405-nm laser (confocal mode). In either mode, begin with a low laser power (e.g., 1% on a Zeiss LSM 780) and pixel dwell time (e.g., 12.6 µs, corresponding to a scanning speed of 5 on a Zeiss LSM 780), and perform a single photoactivation scan across the entire nucleus. A circular region of interest can be configured on most commercial microscopes. Then acquire an image of the embryo using the same settings as those used for the pre-photoactivation image. Assess the efficiency of photoactivation by determining the extent of increase in paGFP fluorescence intensity within the nucleus as compared with that of the pre-photoactivation image. Repeat the photoactivation step with incrementally higher laser power until the cell nucleus displays a discernible increase in paGFP fluorescence intensity.

18| Acquire a short FCS trace (e.g., a few seconds) within the photoactivated nucleus in the embryo and calculate the corresponding ACF, which is usually done automatically by the FCS acquisition software (such as Zen on a Zeiss LSM 780; see Step 27 for more details). Note the count rate and CPM value in the raw trace and the correlation amplitude in the ACF.

19| Repeat Steps 17 and 18 on a different spot of the cell nucleus or inside a fresh cell nucleus of the embryo, using different laser power, pixel dwell time, and number of photoactivation iterations, until a suitable combination is found that produces the most satisfactory count rate, CPM value, and correlation amplitude.
▲ CRITICAL STEP We have empirically found that a count rate in the range of 10–50 kHz and a CPM value >1 kHz produces ACFs with the most satisfactory S/N ratio. We typically obtain a CPM value of 2 kHz or higher in live mouse embryos. Although higher CPM values are generally desirable, care should be taken to ensure that they are not obtained at the expense of photobleaching as a result of using excessively high laser powers. The correlation amplitude should ideally be >1.1; we have found that a correlation amplitude <1.04 results in inaccurate fitting of the ACF.
? TROUBLESHOOTING

20| With the optimized photoactivation parameters, perform a power titration to determine the optimal power for FCS acquisition by first acquiring an FCS trace (e.g., 10 s) on a properly photoactivated nucleus using a low power for the 488-nm laser (e.g., 0.5% on Zeiss LSM 780, or approximately equivalent to 1 µW at the back aperture of the objective), and calculating the corresponding ACF. Note the count rate and CPM value in the raw trace and the correlation amplitude in the ACF.

21| Repeat Step 20 on a different spot or cell nucleus in the embryo using an incrementally higher power for the 488-nm laser, until photobleaching is detectable (as evidenced by a gradual decrease in count rate) over the course of FCS acquisition. The optimal laser power for acquisition should be the value below this threshold that yields the best CPM value and correlation amplitude.

Acquisition of paFCS data ● TIMING ~10 min per experiment
22| Select a new embryo expressing both H2B-RFP and TF-paGFP in the cell nuclei, and acquire an image of the embryo using both the 488- and 568-nm lasers.

23| Photoactivate a cell nucleus of choice using the optimized settings. Check the success of the photoactivation step by acquiring a new image of the embryo with the same settings used for the pre-photoactivation image; the cell nucleus should show visibly increased paGFP fluorescence intensity.

24| Select a location within the photoactivated cell nucleus to perform the FCS measurement, avoiding regions such as nucleoli, where no H2B-RFP is present. Acquire a set of 5–10 FCS traces using the optimized parameters.
▲ CRITICAL STEP Make sure that no discernable photobleaching occurs during the entire acquisition period.
? TROUBLESHOOTING

25| Immediately after FCS measurement, acquire a new image of the embryo using identical settings as those used for the pre- and post-photoactivation images, and compare the new image with those previous images. As an indicator

of the completion of FCS acquisition, a small bleached spot typically appears in the nucleus (e.g., in the H2B-RFP channel, which is relatively immobile) at the position where the laser was parked during FCS acquisition.

26| Repeat Steps 22–25 on as many cell nuclei or embryos as necessary, or on embryos under experimental perturbations (e.g., drug treatment, expression of mutant TF forms). If the embryos are constantly maintained under the stipulated temperature and CO_2 conditions, dozens of cell nuclei can be examined during a single day of experiments.
? TROUBLESHOOTING

Analysis and fitting of paFCS data ● TIMING ~20 min per experiment
27| Open a raw paFCS trace and calculate the corresponding ACF. Typically, such calculation is automatically performed by the FCS acquisition software (such as Zen on a Zeiss LSM 780). If this option is not available, commercial analysis software such as SimFCS (Laboratory of Fluorescence Dynamics), FFS Data Processor (Scientific Software Technology Center, Belarusian State University), and open-source software such as PyCorrFit[50] and QuickFit3 can be used.
▲ CRITICAL STEP Check to make sure that the ACF curves relax to 1 or 0 toward the end of the lag-time range. Failure of this to occur might prevent the accurate fitting of the ACFs.
? TROUBLESHOOTING

28| Discard ACF curves from FCS traces that exhibit abnormalities (e.g., motion-induced artifacts, signs of photobleaching, failure to relax), and perform averaging of the remaining ACF curves. An ultrafast correlation in the vicinity of 1 µs is present mainly because of the after-pulse effect of the avalanche photodetector (APD), and should also not be included for subsequent analysis. In some of the algorithms available for FCS data analysis, such removal of artifacts in defined time windows can be automatically performed[51].

29| Start the fitting procedure by initializing the model parameters. Some parameters for the confocal volume such as structural parameter and lateral waist are obtained from the microscope calibration (see 'Microscope setup and calibration' section), whereas other parameters, such as diffusion time and residence time, can be estimated by visualizing the experimental curves obtained. For example, as diffusion is always faster than binding, diffusion time can be identified as a bump in the ACF between 0.1 and 0.3 ms, whereas the short- and long-lived binding components can be identified as bumps at longer times between 1 and 1,000 ms.

30| Perform fitting of the ACF using the different models outlined above, and calculate the residual as the difference between the fitted curve and the experimental curve at each time point. The shape of the residual curve is useful for detecting failure of the model to fit certain components of the ACF. In general, lower residual values that are symmetrically distributed around zero indicate a better fit.
▲ CRITICAL STEP In the case of the 'two binding components' model (equation (10)), which contains multiple exponential functions, a global fitting routine should be applied to all ACF curves obtained in each FCS experiment, using a common value of k_{off} in order to accurately recover the binding parameters[52].
? TROUBLESHOOTING

31| (Optional) When performing multicomponent fitting, the triplet-state component, which typically falls between 1 and 10 µs for photoactivatable fluorescent proteins such as paGFP, can be excluded from the fitting routine in order to minimize the number of parameters used[53]. Such exclusion is valid when triplet-state formation and diffusion exhibit clear separation of time scales. In such cases, the fitting procedure is applied to the portion of the ACF curve after 10 µs. However, when the particular fluorescent protein used is known to exhibit photodynamics on longer time scales, such exclusion should not be performed.

32| From the various models tested, select the model that best fits the ACF. When the distinction between the various models cannot easily be made, a Bayesian inference procedure based on the S/N ratio of the data sets can be performed to objectively select the most appropriate model while preventing overfitting of the data[54,55]. Such Bayesian testing capability is available in open-source FCS analysis software such as QuickFit3.

33| Once the most suitable model is selected, calculate the mean and standard deviation of the parameters obtained, as well as the mean fit curve. Plot them as appropriate.

? TROUBLESHOOTING
Troubleshooting advice can be found in **Table 1**.

© 2017 Macmillan Publishers Limited, part of Springer Nature. All rights reserved.

TABLE 1 | Troubleshooting table.

Step	Problem	Possible reason	Solution
6	The injection needle is clogged	The RNA prep was not clean enough	Respin the RNA or make a fresh sample
		The needle was not pulled properly	Flush the needle a few times with buffer; if the problem persists, remake the needle using modified pulling parameters (e.g., changing the value of 'pull' and/or 'velocity')
10	The shape of the pinhole alignment curve is not Gaussian	Mismatch of optical filters	Make sure that the optical filters and dichroic mirror are compatible with the dyes used
		Misalignment of pinhole	Recheck the alignment of the pinhole
16	No light is passing through the microscope	The lasers are not turned on, not warmed up, or the shutter is closed	Turn on the laser, wait until it has warmed up, and ensure that the shutter is open
		Filters and dichroic mirror used are incompatible with the fluorescent proteins	Check the components in the light path and modify as necessary
	The embryo drifts in lateral or axial directions	The imaging chamber is not properly mounted on the microscope stage	Adjust or remount the imaging chamber and allow 1 h for the embryos to settle and the culture medium to re-equilibrate with the microscope environment
19	The FCS count rate is too low to obtain satisfactory CPM values, even with repeated photoactivation	Fluorescent protein expression level is too low	Microinject new embryos with higher concentrations of mRNA
		Illumination laser power used is too low	Increase the power of the illumination laser used
		PSF is deformed because of pinhole misalignment	Redo the pinhole alignment
	The FCS count rate is too high to obtain satisfactory CPM values even without photoactivation	Fluorescent protein expression level is too high	Microinject new embryos with lower concentrations of mRNA
24	The count rate decreases over the course of acquisition	Photobleaching has occurred	Reduce the laser power used to minimize photobleaching
26	The embryos show signs of growth arrest or lysis after culture or drug treatments	Culture medium, incubation conditions, or drug treatments have affected their viability	Ensure that all culture medium and incubation conditions are appropriate, or perform titration experiments to rule out unwanted drug-induced defects
	It is not possible to photoactivate mutant TFs	Mutation of the TF has affected its expression or ability to be photoactivated	Re-examine the mutant sequence; if the sequence is as expected, then the particular mutant may not be able to be photoactivated
27	The ACF curves do not relax to 1 or 0 at the end of the correlation time range	The acquisition period is too short	Extend the acquisition period
		Photobleaching has occurred	Reduce the laser power used to minimize photobleaching
		Sample movement has occurred	Pick another cell or embryo that is more immobile and redo the FCS acquisition
30	The ACF analysis produces poor fits	Inappropriate initiation values or model have been used for the data	Reset initiation values based on visual examination of the ACF curve, or use known values
			Use a different or modified model for fitting
	The diffusion parameters obtained from fitting are higher than expected	After-pulsing of the APD detectors are included in the fitting	Remove the after-pulses from the ACF and repeat the fitting
	The diffusion time is as expected, but the diffusion coefficient is not	The confocal volume is not accurately measured	Repeat the measurement of the confocal volume and recalculate the diffusion parameters

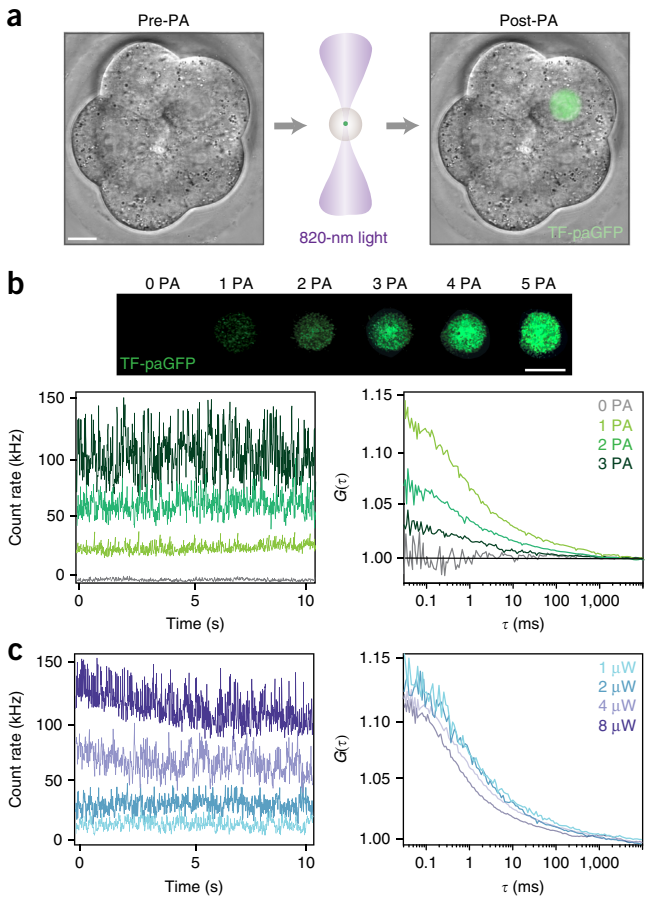

Figure 2 | Selective photoactivation of a TF subpopulation and optimization of photoactivation and paFCS acquisition parameters. (**a**) Representative images of a live, eight-cell mouse embryo expressing a paGFP-tagged TF before (left) and after (right) a single cell nucleus is selectively photoactivated (green circle) with an 820-nm multiphoton laser. (**b**) An example of the effect of iterative photoactivation (PA) steps on the quality of ACF curves. In this case, although repeated photoactivation increases the fraction of TF-paGFP molecules activated (top) and the count rate in raw FCS traces (bottom left), the correlation amplitude in the ACF curve decreases as the number of PA steps is increased from 1 to 3 (bottom right). The optimal number of iterations to be used here is therefore 1. (**c**) Tuning of the laser power for FCS data acquisition to achieve optimum ACF quality without noticeable photobleaching. In this case, as laser power is increased from 1 to 8 µW, gradual photobleaching can be discerned in the FCS traces (left) while the ACF curve exhibits photobleaching-related shift starting at 4 µW (right). The optimal power to be used here is therefore 2 µW. Scale bar, 10 µm. **b** and **c** adapted with permission from ref. 27, Nature Publishing Group.

● TIMING

Steps 1–7, embryo isolation, culture, and pro-nuclear microinjection: ~1 d
Steps 8–12, microscope calibration: ~1 h
Steps 13–16, setup of the microscope for paFCS: ~1.5 h
Steps 17–21, optimization of photoactivation and acquisition parameters: ~30 min
Steps 22–26, acquisition of paFCS data: ~10 min per experiment
Steps 27–33, analysis and fitting of paFCS data: ~20 min per experiment

ANTICIPATED RESULTS

The process of selectively photoactivating a paGFP-tagged TF (in this case Sox2) subpopulation in a live mouse embryo is shown in **Figure 2a**. To illustrate the optimization of the photoactivation and FCS acquisition parameters, **Figure 2b**,**c** shows how the count rate and the quality of the ACF depend on the number of photoactivation iterations, as well as on the acquisition laser power used. For Sox2-paGFP in mouse embryos, when using 10% laser power for each photoactivation step, the optimal number of photoactivation iterations is one, as further photoactivation excites too many Sox2-paGFP molecules, thereby deteriorating the ACF quality (**Fig. 2b**). As for acquisition, increasing the 488-nm laser power from 1 to 2 µW improves the quality of the ACF; however, further increase to 4 µW and beyond leads to photobleaching and photobleaching-associated artifacts (**Fig. 2c**).

Representative images of a cell nucleus in a live mouse embryo before and after photoactivation, as well as after paFCS data acquisition, are shown in **Figure 3a**. The continuous illumination during paFCS acquisition causes bleaching of some of the H2B-RFP molecules in the cell nucleus, but such a bleaching effect is not observed in the Sox2-paGFP channel because of the rapid replenishing of bleached molecules by the freely diffusing Sox2 molecules

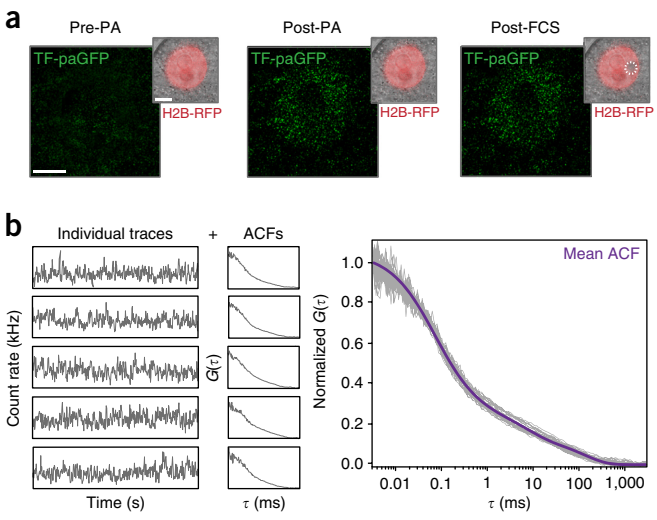

Figure 3 | Acquisition of fluorescence intensity fluctuation traces and ACF curves. (**a**) Representative images of a cell nucleus in a live mouse embryo before (left) and after (middle) photoactivation, and after paFCS data acquisition (right). The level of photoactivation shown in the middle panel is found to be optimal for acquiring paFCS data with a high S/N ratio. The white dotted circle in the inset of the right panel indicates the region bleached during paFCS acquisition. (**b**) Typical raw fluctuation traces (left), the corresponding ACF curves (middle), and the mean ACF curve (right, purple line) obtained from a single paFCS experiment. Scale bars, 5 µm.

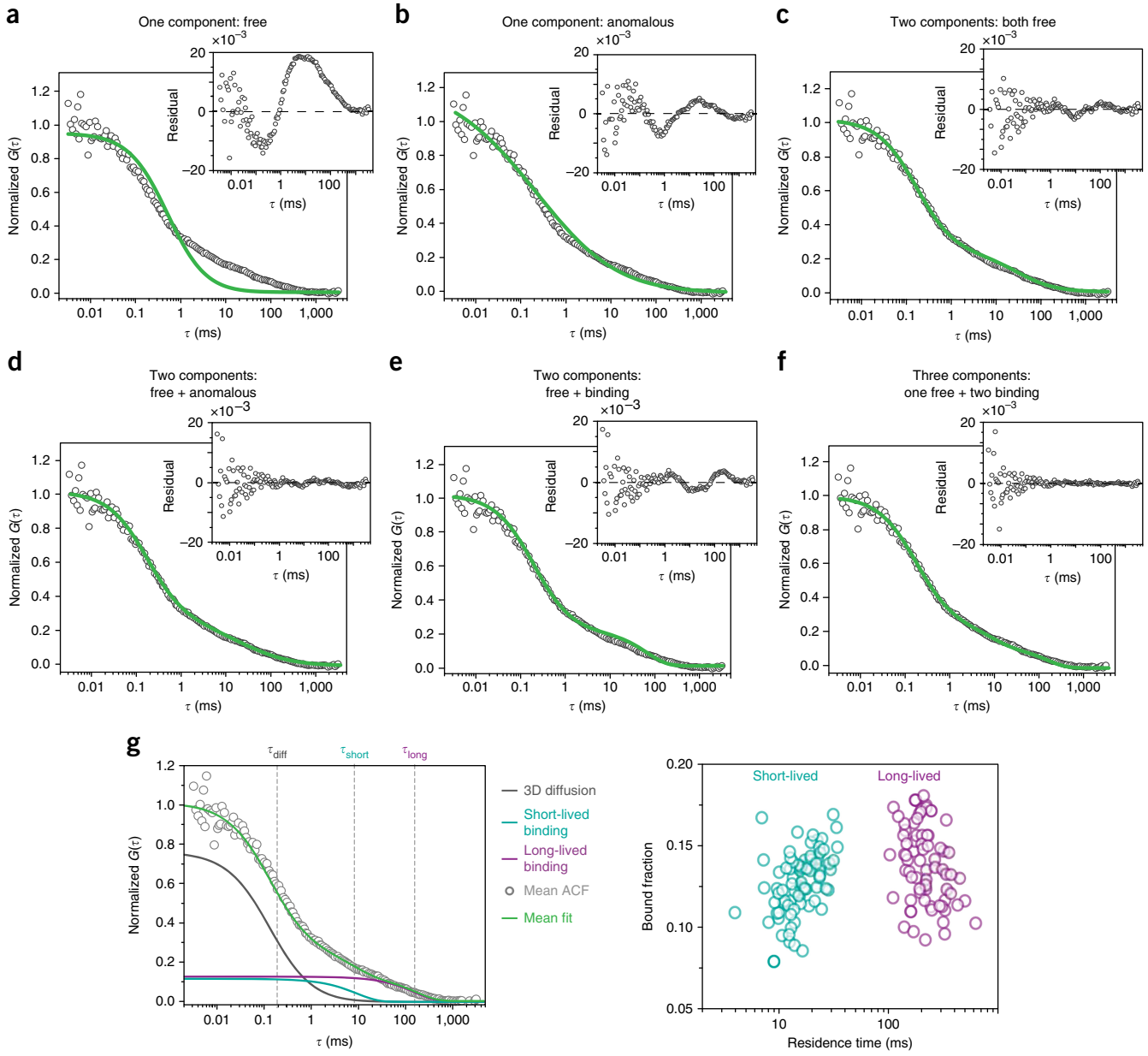

Figure 4 | Model selection for fitting paFCS data. (**a**–**f**) Various models used to fit ACF curves, incorporating (**a**) one free diffusion component; (**b**) one anomalous diffusion component; (**c**) two free diffusion components; (**d**) one free diffusion component and one anomalous diffusion component; (**e**) one free diffusion component and one binding component; and (**f**) one free diffusion component and two binding components. In this case, the model in **f** produces the best fit for the experimental data. (**g**) Using the model in **f** for fitting the experimental ACFs of Sox2-paGFP resolves two subpopulations in addition to free diffusion (left) with distinct residence times (right), corresponding to short- and long-lived DNA binding, respectively. Each circle in the right panel denotes a single cell. **a**–**d** adapted with permission from ref. 27, Nature Publishing Group. **g** adapted with permission from ref. 28, Cell Press.

in the nucleoplasm. **Figure 3b** shows the results of a typical paFCS experiment, consisting of a set of 5 raw fluctuation traces, corresponding ACF curves, and the mean ACF curve calculated from the raw curves.

The fitting process for ACF curves obtained from the above experiment is illustrated in **Figure 4**. Models with only one component of free or anomalous diffusion do not provide satisfactory fits to the experimental ACF (**Fig. 4a**,**b**), and call for the simultaneous incorporation of two diffusion components, either both free (**Fig. 4c**) or one free and one anomalous (**Fig. 4d**). Both models fit the experimental data better (with lower residuals) than with the 'one-component' models. However, the 'two free components' model still exhibits fluctuations in ACF residuals in the 1- to 100-ms regime, and may be more suitable for molecular species with a subpopulation that diffuses much more slowly than the free component[56].

Moreover, a model that accounts for both diffusion and binding to chromatin using one diffusive and one binding component still shows substantial fitting residual (**Fig. 4e**), whereas a model containing two binding components and one diffusive

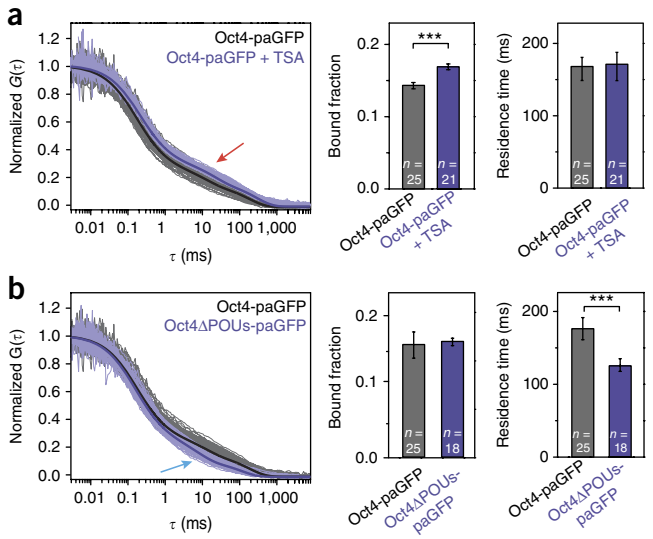

Figure 5 | Probing the impact of mutation and drug treatment on TF-binding dynamics with paFCS. (**a**) TSA treatment causes a rightward shift of ACF curve (left, red arrow), an increase in the long-lived bound fraction (middle), but no significant change in the residence time (right) of Oct4-paGFP. (**b**) Truncation of the POU-specific DNA-binding domain of Oct4 (Oct4ΔPOUs-paGFP) causes a leftward shift of the ACF curve (left, blue arrow), no change in the long-lived bound fraction (middle), but a reduction in the residence time (right) of Oct4-paGFP. Data are presented as mean ± s.e.m.; *n*, number of cells; *P* values are determined by Student's *t* test; ***$P < 0.001$. **b** (left part) adapted with permission from ref. 27, Nature Publishing Group.

component results in excellent fitting (**Fig. 4f**). Using this model, two distinct modes of TF–DNA interaction, short-lived and long-lived binding, can be distinguished based on their markedly different residence times (**Fig. 4g**).

paFCS can be used to quantitatively probe changes in the DNA-binding dynamics of a TF induced by molecular manipulations, cell differentiation, or differential gene expression. For example, when treated with TSA, the long-lived bound fraction of Oct4-paGFP is found to be significantly increased, whereas the residence time remains relatively unchanged, as a result of increased DNA accessibility induced by the drug (**Fig. 5a**). On the other hand, a truncated form of Oct4-paGFP, in which the POU-specific DNA-binding domain of Oct4 is deleted (Oct4ΔPOUs-paGFP), exhibits reduced residence time without change in the bound fraction as compared with that of wild-type Oct4-paGFP, because of the mutant's impaired DNA-binding capability (**Fig. 5b**).

ACKNOWLEDGMENTS We thank J. Silva for help with embryo isolation and microinjection, and V. Levi for advice on modeling. This work was supported by an A*STAR National Science Scholarship (to Z.W.Z.), a Human Frontiers Science Program Fellowship (to J.Z.), and an A*STAR Investigatorship and EMBO Young Investigator grants (to N.P.).

AUTHOR CONTRIBUTIONS N.P. conceived the project; Z.W.Z. and Y.D.A. performed the microscope calibration, optimization of photoactivation/acquisition parameters, and paFCS measurements; M.D.W. and J.Z. performed drug treatment and mutant TF experiments. Y.D.A. performed data analysis and modeling. S.B. performed embryo isolation, culture, and mRNA microinjections. Z.W.Z., M.D.W., Y.D.A., J.Z., S.B. and N.P. wrote the manuscript.

COMPETING FINANCIAL INTERESTS The authors declare no competing financial interests.

1. McNally, J.G., Müller, W.G., Walker, D., Wolford, R. & Hager, G.L. The glucocorticoid receptor: rapid exchange with regulatory sites in living cells. *Science* **287**, 1262–1265 (2000).
2. Gebhardt, J.C.M. *et al.* Single-molecule imaging of transcription factor binding to DNA in live mammalian cells. *Nat. Methods* **10**, 421–426 (2013).
3. Mueller, F., Wach, P. & McNally, J.G. Evidence for a common mode of transcription factor interaction with chromatin as revealed by improved quantitative fluorescence recovery after photobleaching. *Biophys. J.* **94**, 3323–3339 (2008).
4. Morisaki, T., Müller, W.G., Golob, N., Mazza, D. & McNally, J.G. Single-molecule analysis of transcription factor binding at transcription sites in live cells. *Nat. Commun.* **5**, 4456 (2014).
5. Chen, J. *et al.* Single-molecule dynamics of enhanceosome assembly in embryonic stem cells. *Cell* **156**, 1274–1285 (2014).
6. Mazza, D., Abernathy, A., Golob, N., Morisaki, T. & McNally, J.G. A benchmark for chromatin binding measurements in live cells. *Nucleic Acids Res.* **40**, e119 (2012).
7. Sugo, N. *et al.* Single-molecule imaging reveals dynamics of CREB transcription factor bound to its target sequence. *Sci. Rep.* **5**, 10662 (2015).
8. Speil, J. *et al.* Activated STAT1 transcription factors conduct distinct saltatory movements in the cell nucleus. *Biophys. J.* **101**, 2592–2600 (2011).
9. Liu, Z. *et al.* 3D imaging of Sox2 enhancer clusters in embryonic stem cells. *eLife* **3**, e04236 (2014).
10. Izeddin, I. *et al.* Single-molecule tracking in live cells reveals distinct target-search strategies of transcription factors in the nucleus. *eLife* **3**, e02230 (2014).
11. Zhao, Z.W., White, M.D., Bissiere, S., Levi, V. & Plachta, N. Quantitative imaging of mammalian transcriptional dynamics: from single cells to whole embryos. *BMC Biol.* **14**, 115 (2016).
12. Hager, G.L., McNally, J.G. & Misteli, T. Transcription dynamics. *Mol. Cell* **35**, 741–753 (2009).
13. Voss, T.C. & Hager, G.L. Dynamic regulation of transcriptional states by chromatin and transcription factors. *Nat. Rev. Genet.* **15**, 69–81 (2014).
14. Coleman, R.A. *et al.* Imaging transcription: past, present, and future. *Cold Spring Harb. Symp. Quant. Biol.* **80**, 1–8 (2015).
15. Darzacq, X. *et al.* Imaging transcription in living cells. *Annu. Rev. Biophys.* **38**, 173–196 (2009).
16. Magde, D., Elson, E. & Webb, W.W. Thermodynamic fluctuations in a reacting system-measurement by fluorescence correlation spectroscopy. *Phys. Rev. Lett.* **29**, 705–708 (1972).
17. Elson, E.L. Fluorescence correlation spectroscopy: past, present, future. *Biophys. J.* **101**, 2855–2870 (2011).
18. Macháň, R. & Wohland, T. Recent applications of fluorescence correlation spectroscopy in live systems. *FEBS Lett.* **588**, 3571–3584 (2014).
19. Digman, M.A. & Gratton, E. Lessons in fluctuation correlation spectroscopy. *Annu. Rev. Phys. Chem.* **62**, 645–668 (2011).
20. Weidemann, T., Mücksch, J. & Schwille, P. Fluorescence fluctuation microscopy: a diversified arsenal of methods to investigate molecular dynamics inside cells. *Curr. Opin. Struct. Biol.* **28**, 69–76 (2014).
21. Bacia, K. & Schwille, P. Practical guidelines for dual-color fluorescence cross-correlation spectroscopy. *Nat. Protoc.* **2**, 2842–2856 (2007).
22. Krieger, J.W. *et al.* Imaging fluorescence (cross-) correlation spectroscopy in live cells and organisms. *Nat. Protoc.* **10**, 1948–1974 (2015).
23. Rossow, M.J., Sasaki, J.M., Digman, M.A. & Gratton, E. Raster image correlation spectroscopy in live cells. *Nat. Protoc.* **5**, 1761–1774 (2010).
24. Weidemann, T. Application of fluorescence correlation spectroscopy (FCS) to measure the dynamics of fluorescent proteins in living cells. in *Fluorescence Spectroscopy and Microscopy: Methods and Protocols* (eds. Engelborghs, Yves & Visser, Antonie J.W.G.) 539–555 (Humana Press, 2014).
25. Biggin, M.D. Animal transcription networks as highly connected, quantitative continua. *Dev. Cell* **21**, 611–626 (2011).
26. Patterson, G.H. & Lippincott-Schwartz, J. A photoactivatable GFP for selective photolabeling of proteins and cells. *Science* **297**, 1873–1877 (2002).

27. Kaur, G. *et al.* Probing transcription factor diffusion dynamics in the living mammalian embryo with photoactivatable fluorescence correlation spectroscopy. *Nat. Commun.* **4**, 1637 (2013).
28. White, M.D. *et al.* Long-lived binding of Sox2 to DNA predicts cell fate in the four-cell mouse embryo. *Cell* **165**, 75–87 (2016).
29. Zhao, Z.W., Gebhardt, J.C.M., Suter, D.M. & Xie, X.S. Reply to 'Convergence of chromatin binding estimates in live cells'. *Nat. Methods* **10**, 692 (2013).
30. Wang, Y., Wang, X., Wohland, T. & Sampath, K. Extracellular interactions and ligand degradation shape the nodal morphogen gradient. *eLife* **5**, e13879 (2016).
31. Yu, S.R. *et al.* Fgf8 morphogen gradient forms by a source-sink mechanism with freely diffusing molecules. *Nature* **461**, 533–536 (2009).
32. Shi, X. *et al.* Determination of dissociation constants in living zebrafish embryos with single wavelength fluorescence cross-correlation spectroscopy. *Biophys. J.* **97**, 678–686 (2009).
33. Capoulade, J., Wachsmuth, M., Hufnagel, L. & Knop, M. Quantitative fluorescence imaging of protein diffusion and interaction in living cells. *Nat. Biotech.* **29**, 835–839 (2011).
34. Wohland, T., Shi, X., Sankaran, J. & Stelzer, E.H.K. Single plane illumination fluorescence correlation spectroscopy (SPIM-FCS) probes inhomogeneous three-dimensional environments. *Opt. Express* **18**, 10627–10641 (2010).
35. Digman, M.A. *et al.* Measuring fast dynamics in solutions and cells with a laser scanning microscope. *Biophys. J.* **89**, 1317–1327 (2005).
36. Digman, M.A. & Gratton, E. Imaging barriers to diffusion by pair correlation functions. *Biophys. J.* **97**, 665–673 (2009).
37. Ries, J., Chiantia, S. & Schwille, P. Accurate determination of membrane dynamics with line-scan FCS. *Biophys. J.* **96**, 1999–2008 (2009).
38. Pantazis, P. & González-Gaitán, M. Localized multiphoton photoactivation of paGFP in *Drosophila* wing imaginal discs. *J. Biomed. Opt.* **12**, 044004 (2007).
39. Plachta, N., Bollenbach, T., Pease, S., Fraser, S.E. & Pantazis, P. Oct4 kinetics predict cell lineage patterning in the early mammalian embryo. *Nat. Cell Biol.* **13**, 117–123 (2011).
40. Wang, S., Moffitt, J.R., Dempsey, G.T., Xie, X.S. & Zhuang, X. Characterization and development of photoactivatable fluorescent proteins for single-molecule–based superresolution imaging. *Proc. Natl. Acad. Sci. USA* **111**, 8452–8457 (2014).
41. Mohr, M.A., Argast, P. & Pantazis, P. Labeling cellular structures *in vivo* using confined primed conversion of photoconvertible fluorescent proteins. *Nat. Protoc.* **11**, 2419–2431 (2016).
42. Rigler, R., Mets, Ü., Widengren, J. & Kask, P. Fluorescence correlation spectroscopy with high count rate and low background: analysis of translational diffusion. *Eur. Biophys. J.* **22**, 169–175 (1993).
43. Widengren, J., Mets, Ü. & Rigler, R. Photodynamic properties of green fluorescent proteins investigated by fluorescence correlation spectroscopy. *Chem. Phys.* **250**, 171–186 (1999).
44. Halford, S.E. & Marko, J.F. How do site-specific DNA-binding proteins find their targets? *Nucleic Acids Res.* **32**, 3040–3052 (2004).
45. Michelman-Ribeiro, A. *et al.* Direct measurement of association and dissociation rates of DNA binding in live cells by fluorescence correlation spectroscopy. *Biophys. J.* **97**, 337–346 (2009).
46. Elson, E.L. Brief introduction to fluorescence correlation spectroscopy. in *Methods in Enzymology* Vol. 518 (ed. Tetin, S.Y.), 11–41 (Academic Press, 2013).
47. Sobell, H.M. Actinomycin and DNA transcription. *Proc. Natl. Acad. Sci. USA* **82**, 5328–5331 (1985).
48. Yoshida, M., Horinouchi, S. & Beppu, T. Trichostatin A and trapoxin: novel chemical probes for the role of histone acetylation in chromatin structure and function. *BioEssays* **17**, 423–430 (1995).
49. Behringer, R., Gertsenstein, M., Nagy, K.V. & Nagy, A. *Manipulating the Mouse Embryo: A Laboratory Manual* 4th ed. (Cold Spring Harbor Laboratory Press, 2014).
50. Müller, P., Schwille, P. & Weidemann, T. PyCorrFit—generic data evaluation for fluorescence correlation spectroscopy. *Bioinformatics* **30**, 2532–2533 (2014).
51. Ries, J. *et al.* Automated suppression of sample-related artifacts in fluorescence correlation spectroscopy. *Opt. Express* **18**, 11073–11082 (2010).
52. Beechem, J.M. Global analysis of biochemical and biophysical data. in *Methods Enzymol.* Vol. 210, 37–54 (Academic Press, 1992).
53. Wachsmuth, M., Waldeck, W. & Langowski, J. Anomalous diffusion of fluorescent probes inside living cell nuclei investigated by spatially-resolved fluorescence correlation spectroscopy. *J. Mol. Biol.* **298**, 677–689 (2000).
54. He, J., Guo, S.-M. & Bathe, M. Bayesian approach to the analysis of fluorescence correlation spectroscopy data I: theory. *Anal. Chem.* **84**, 3871–3879 (2012).
55. Sun, G. *et al.* Bayesian model selection applied to the analysis of fluorescence correlation spectroscopy data of fluorescent proteins *in vitro* and *in vivo*. *Anal. Chem.* **87**, 4326–4333 (2015).
56. Schwille, P., Bieschke, J. & Oehlenschläger, F. Kinetic investigations by fluorescence correlation spectroscopy: the analytical and diagnostic potential of diffusion studies. *Biophys. Chem.* **66**, 211–228 (1997).